Available online at www.sciencedirect.com
ScienceDirect
Renewable and Sustainable Energy Reviews
12 (2008) 2301–2330
RENEWABLE & SUSTAINABLE ENERGY REVIEWS
www.elsevier.com/locate/rser

Review of modeling details related to renewably powered hydrogen systems

Sachin S. Deshmukh, Robert F. Boehm*

Center for Energy Research, University of Nevada, Las Vegas NV 89154-4027, USA

Received 7 May 2007; accepted 20 June 2007

Abstract

This paper provides a detailed review of renewably driven hydrogen systems and modeling approaches applicable to these systems that have been reported over the last two decades. Several renewable energy technologies, including solar photovoltaic, wind, and hydro, have been considered as the power source in these reports. Storage is an important aspect of hydrogen systems, and options for this are summarized here. Utilization systems include fuel cells as well as a variety of thermal uses. Some of the reported studies have addressed residential applications whereas others were related to commercial scale systems. This paper particularly emphasizes aspects of modeling of the various components for the renewable hydrogen system. Based on the literature on this area, conclusions are provided on the current understanding as well as future work related to this topic.

Keywords: Renewable; Hydrogen; System; Modeling; Energy; Solar

Contents

*Corresponding author. Tel.: +1 702 895 4160; fax: +1 702 895 3936.
E-mail address: boehm@me.unlv.edu (R.F. Boehm).

1364-0321/$ - see front matter
doi:10.1016/j.rser.2007.06.008

1. Introduction

As concerns grow about degradation of the environment, availability of conventional fuels, and the political viability of nuclear power, alternatives for energy supplies need to be examined. One of the hopes for the future is that renewably based approaches for energy can be used as replacements for our currently more-widely used sources. However, many of the renewable energy sources have some degree of temporal output, causing problems for power-on-demand requirements. For this reason, some form of storage will undoubtedly be of value. Also, there will be some future requirements for a transportable fuel that may or may not be able to be satisfied by batteries.

One approach to be considered is use of hydrogen as a significant element in our energy future. Major advantages of using hydrogen include: firstly, it is a clean source of energy; secondly, it can be used for seasonal storage of energy; thirdly, it can be transported (say as an aircraft fuel), and finally it can be used to produce electrical as well as thermal forms of energy.

The concept of integrating renewable energy with hydrogen systems was given some serious consideration in the 1970s [1,2]. Fischer [3] provided an interesting review on experimental and analytical studies of early photovoltaic/electrolyzer systems used for hydrogen production. Most of the experimental studies reported were on a laboratory scale.

In last three decades, intense research has been conducted around the world on this topic. Emphases are not only to improve the performance of existing hydrogen production, storage and utilization technologies, but also to integrate them effectively with renewable energy sources. As noted above, one of the key elements of this is that it provides a good buffer to time-varying energy inputs.

Fig. 1 shows a generic renewable hydrogen system. The renewable energy source can be of any type, including time-varying forms such as solar, wind, and hydroelectric. Hydrogen can be produced by electricity from these kinds of systems as well as by chemical and biological means [4].

Storage is an important aspect of this type of system. This is particularly true if this is driven by a time-varying energy source but it is also needed if there is a widely varying time

Nomenclature

A_{pv}	area of PV module (m^2)
a	modified ideality factor ($a = n_{pv}kT_{pv}N_s/q$)
a_c, b_c	empirical constants for cell temperature calculation
A_{fc}	active area of cell (cm^2)
age	operation time for fuel cell (h)
a_{ref}	reference modified ideality factor
c^*_{H+}	proton concentration at the cathode membrane/gas interface (mol/cm^3)
$c^*_{H_2}$	liquid-phase concentration of hydrogen at the anode/gas interface (mol/cm^3)
$c^*_{H_2O}$	water concentration at the cathode membrane/gas interface (mol/cm^3)
$c^*_{O_2}$	concentration of oxygen at cathode membrane/gas interface (mol/cm^3)
C_{cw}	thermal capacity of cooling water (J/K)
C_{mh}	effective heat capacity (J/°C)
C_p	specific heat at constant pressure (J/mol K)
$C_{t,el}$	overall heat capacity of electrolyzer (J/K)
F	Faraday's number (96485)
G_{NOCT}	instantaneous solar irradiation at SRC (W/m^2)
G_T	instantaneous total solar irradiation on PV (W/m^2)
i	current density draw from fuel cell (A/cm^2)
I_{el}	electrolyzer current (A)
$I_{L,ref}$	reference light current (A)
I_L	light current (A)
i_L	maximum current density (A/cm^2)
$I_{m,ref}$	reference maximum power point current of PV cell (A)
I_m	maximum power point current of PV cell (A)
$I_{O,ref}$	reference diode reverse saturation current (A)
I_O	diode reverse saturation current (A)
I_{pv}	current of PV cells (A)
$I_{sc,ref}$	reference short circuit current (A)
I_{sc}	short circuit current (A)
k	Boltzmann's constant (1.381×10^{-23} J/K)
k_a^0, k_c^0	reaction rate constants for anode and cathode, respectively (cm/s)
k_{cell}	empirical term to represent the apparent rate constant for anode and cathode
k_{DR}	empirical term to represent the change in catalytic activity with age (V/h K)
k_{eff}	effective heat loss coefficient (W/°C)
L	membrane thickness (cm)
$LMTD$	log mean temperature difference for heat exchanger (K)
n	number of electrons transferred per reaction (2)
n_c	number of electrons involved in the reaction
$N_{c,el}$	number of cells in electrolyzer stack
$N_{c,fc}$	number of cells in fuel cell stack
n_{gas}	hydrogen flow rate (mol/s)
$\dot{n}_{H_2}$	molar flow rate of hydrogen (mol/s)

$\dot{n}_{H_2O}$	molar flow rate of water (mol/s)
$\dot{n}_{O_2}$	molar flow rate of oxygen (mol/s)
n_{poly}	polytropic index
n_{pv}	parameter
N_s	number of cells in series
n_{st}	number of moles of hydrogen inside the storage tank (mol)
p	operating pressure of electrolyzer cell (N/m^2)
$P_{a,\ ht}$	actual available power of hydro turbine (W)
$P_{a,\ wt}$	actual available power of wind turbine (W)
$p_{c,in}$	pressure at the outlet of compressor (N/m^2)
$p_{c,out}$	pressure at the outlet of compressor (N/m^2)
P_{comp}	power required by compressor (W)
p_{eq}	equilibrium pressure of hydrogen gas (N/m^2)
P_{H2}	partial pressure of hydrogen (N/m^2)
P_{O2}	partial pressure of oxygen (N/m^2)
P_{ref}	reference pressure (N/m^2)
p_{st}	pressure inside the storage tank (N/m^2)
$P_{th,\ wt}$	theoretical available power of wind turbine (W)
q	electronic charge (1.609×10^{-19} A s)
Q_{cool}	heat lost to cooling media (W)
Q_{gen}	heat generated by elecrolyzer (W)
Q_{loss}	heat loss (convection and radiation to ambient) by electrolyzer (W)
Q_{mh}	total heat production/consumption (W)
R	gas constant
r_1, r_2, s, t_1, t_2, t_3	empirical constants for electrolyzer
$R^{electronic}$	resistance to flow of electrons at the electrodes (Ω)
r_m	membrane specific resistivity for the flow of hydrated protons (Ω cm)
R^{proton}	resistance to the flow of protons in the cell (Ω)
$R_{s,ref}$	reference series resistance (Ω)
R_s	series resistance (Ω)
$R_{sh,ref}$	reference shunt resistance (Ω)
R_{sh}	shunt resistance (Ω)
$R_{t,el}$	overall thermal resistance of electrolyzer (W/K)
$S_{pv,ref}$	reference effective absorbed solar irradiation (W/m^2)
S_{pv}	effective absorbed solar irradiation (W/m^2)
T	operating cell temperature (K)
$T_{a,NOCT}$	ambient temperature at SRC (K)
T_a	ambient temperature (K)
$T_{cw,i}$	cooling water temperature at inlet (K)
$T_{cw,o}$	cooling water temperature at outlet (K)
$T_{m,pv}$	back surface temperature of PV module (K)
T_{NOCT}	cell temperature at standard rated condition (SRC) (K)
T_{pv}	cell temperature of PV (K)
T_{ref}	reference temperature (K)
U_0	standard cell potential (V)
$U_{0,fc}$	standard cell potential for fuel cell (V)

UA_{hx}	product of overall heat transfer coefficient and area of for heat exchanger (W/K)
U_{el}	cell potential for electrolyzer (V)
U_{fc}	overall cell potential for fuel cell (V)
$U_{L,NOCT}$	overall heat transfer (convection and radiation) coefficient of PV at SRC (W/m^2K)
U_L	overall heat transfer (convection and radiation) coefficient of PV (W/m^2K)
$U_{m,ref}$	reference maximum power point voltage of PV cell (V)
U_m	maximum power point voltage of PV cell (V)
$U_{oc,ref}$	reference open-circuit voltage (V)
U_{oc}	open-circuit voltage (V)
U_{pv}	voltage of PV cells (V)
U_{rev}	reversible cell potential (V)
U_{tn}	thermo-neutral potential (V)
V_{st}	volumetric capacity of storage tank (m^3)
WS	wind speed (m/s)
$\alpha, \beta, \gamma, \delta, \varepsilon$	empirical constants for calculation of specific heat at constant pressure
α_c	chemical activity parameter for the cathode
ΔG	change in Gibbs free energy (J/mol)
ΔG_e	standard state free energy of the cathode reaction (J/mol)
ΔG_{ec}	standard state free energy of chemisorption from the gas state (J/mol)
ΔH	change in enthalpy of formation (J/mol)
ΔH^o	standard ($10^5\,N/m^2$ and 298 K) enthalpy of formation (J/mol)
ΔS	change in entropy of formation (J/mol K)
ΔS^o	standard ($10^5\,N/m^2$ and 298 K) entropy of formation (J/mol K)
ΔT_{pv}	temperature difference between cell and module back surface at a 1000 W/m^2 irradiance (°C)
η_{act}	activation losses (V)
$\eta_{c,pv}$	module efficiency to convert incident solar irradiation to electrical energy
η_{comp}	compressor efficiency
η_{conc}	concentration losses (V)
η_{ohm}	ohmic losses (V)
$\xi_1, \xi_2, \xi_3, \xi_4$	empirical parameters for fuel cell

variation of use. This can be accomplished using compressed gas storage tanks, liquefied hydrogen storage, metal hydrides or carbon-based materials. We also consider short-term electrical storage as an option. This could be batteries or grid connection, if the latter is available.

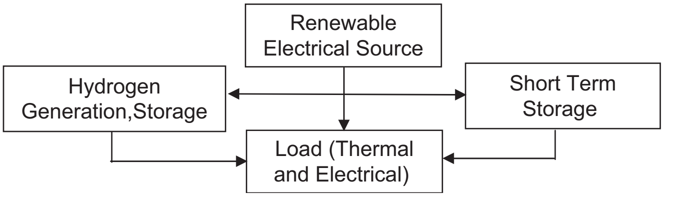


Fig. 1. Generic renewable hydrogen system.

Loads for houses can be classified on an electrical or thermal basis. Electrical loads can be satisfied by fuel cells (stationary and automobile application) whereas hydrogen can be combusted for satisfying thermal loads, e.g., IC engines (cars), cooking, water heating, HVAC systems, etc.

A variety of studies that have been performed on combined renewable energy and hydrogen systems can broadly be classified as follows.

1.1. Renewable hydrogen generation system (RHGS)

The system generates hydrogen from renewable energy sources and can be either stand alone or grid connected. This system is a typical hydrogen refueling station. Note that for residential applications such a system can fulfill the hydrogen requirements for fuel purposes only. A description has been given for the initial design, operation and cost optimization of the system with photovoltaic cells connected to an electrolyzer [5–9]. Experimental data on small-scale systems with proton exchange membrane (PEM) electrolyzers have been summarized [10]. Experimental data for RHGS with PV that was installed on a house in Switzerland have been reported [11].

One of the first studies including description of component models to simulate the performance of the RHGS was given by Carpetis [12]. Others have described simulations performed on the TRNSYS software for similar systems [13]. Hydrogen production as a function of maximum power point and tilt angle has been given. The performance modeling of the RHGS (with PV) was reported [14]. Further, cost optimization studies of a photovoltaic electrolyzer system using HYSOLAR along with performance simulations were reported by Seigel and Schott [15]. Other cost optimization studies have also appeared in the literature [16,17].

Some of the fairly recent studies discussed the preliminary system design and economic feasibility of a combined PV and PEM electrolyzer [18,19]. Bilgen developed models to study performance and cost optimization of PV electrolyzer systems [20]. The paper reported comparisons for fixed and tracking panels. Others have reported the optimum hydrogen cost for a small-scale (<100 W) directly connected RHGS with PV [21]. Another study has focused on the use of PSCAD/EMTDC software for the design and simulation of transient performance of RHGS with PV [22].

1.2. Renewable hydrogen generation and utilization system (RHGUS)

This system not only generates hydrogen from renewable energy sources, but also includes a load that utilizes hydrogen. The load this system serves could be electrical and/or thermal in nature. The system can be either stand alone or grid connected. Such a system includes on-site/off-site hydrogen generation also. The latter refers to a system in which hydrogen is generated at a renewable source facility and transported by some means to the point of use.

Design considerations based on efficiencies and energy calculations for various components of RHGUS with PV as an energy source were reported [23,24]. The long-term operating experience for large-scale demonstration plants of RHGUS systems installed in Germany has been described [25,26]. Griebhaber summarized the energy consumed and generated for RHGUS installed on self-sufficient Solar House [27]. The

efficiencies for various components of RHGUS that supplied continuous power to an air compressor have been noted [28]. Experimental data for the performance of a combined PV and wind turbine-operated RHGUS for remote applications were summarized. A programmable load was used to provide the energy demand for the house [29]. Others reported the performance of RHGUS with PV installed to supply continuous power (200 W) for a remote application. A metal hydride bed was used to store the hydrogen generated by an electrolyzer [30].

Models were developed and overall system simulations were performed to optimize the size of PV array area for the RHGUS system [31]. The program H2PHOTO was developed and simulations were performed based on simple models (electrical and thermal) to design and predict the performance of 1.3 kW RHGUS system [32]. TRNSYS was used to simulate the annual performance of RHGUS system for residential purposes. A catalytic burner was used for providing heat to the house but the sizing of the components depends on both the electrical and thermal loads of the house [33]. Vosen and Keller [34] described time dependent annual simulations for the RHGUS with PV for stand-alone applications using state of charge and neural network control systems. The cost comparison between hydrogen only, battery only and combined system was also provided. Others developed a model to estimate hourly solar radiation on a tilted surface from monthly average daily insolation. This was further used to estimate the energy available from a PV (model based on efficiencies) and wind turbine combined power source for a RHGUS [35]. The RHGUS system for stand-alone residential application was simulated for PV only, PV–micro-hydro turbine and combined PV, wind and micro-hydro turbine as energy sources [36,37]. A thermo-economic analysis was performed for RHGUS with PV [38]. The optimization to minimize the investment cost of RHGUS with PV and micro-hydro turbine was carried out [39]. The results gave local minima but it was not sure that the model gave global minima. Short-term performance of the RHGUS with PV and wind turbine for the control system and power conditioning devices developed by authors was also reported [40]. For the similar system, the effect of operation of electrolyzer with oxygen recovery on the performance of overall system has been described [41]. The dynamic models of various components of RHGUS with PV and wind turbine were developed and compared with experimental results. Further, these models were used to simulate the system performance for residential purposes [42]. The importance of the control strategies, based on simulations performed on TRNSYS, to operate the RHGUS with PV has been noted [43]. Annual simulation for RHGUS with PV and wind turbine was performed for an average load of 1 kW using Hybrid2 software developed by National Renewable Energy Laboratory (NREL) [44]. Performance simulation of the RHGUS system with PV and reformer, installed in Stockholm, Sweden, to obtain hydrogen from biogas has been outlined in the literature [45]. Shapiro et al. reported the performance of an electrolyzer (up to 200 psig) placed inside the storage tank that can be combined with RHGUS [46]. Dynamic modeling of hydrogen side (electrolyzer, storage, and fuel cell) of RHGUS has been performed for application for residential application when combined with PV array [47]. The annual performance modeling of RHGUS with PV for a standard residential house in Las Vegas, NV has been performed by Deshmukh and Boehm [48]. The hydrogen needed for fuelling the automobile and other residential usage (water heating, clothes drying, cooking, etc.) has been considered.

2. Modeling by component

This section reviews various approaches to modeling of various aspects of renewable hydrogen systems. Models considered are based upon their applicability for system simulation purposes. Both components and input phenomena are included here.

2.1. Input resources and hourly data

Modeling of various components requires a variety of input data. Hourly averaged annual data for solar irradiation, temperature, wind speed, wind direction, and water flow are generally needed for modeling.

The hourly averaged solar irradiation data for US can be found on Renewable Resource Data Center developed by NREL [49]. Wind data can be downloaded from the NREL website [50]. Monthly wind rose chart information averaged over thirty years can be obtained from United States Department of Agriculture website [51]. This can be helpful for the design of wind turbine applications for a particular location. For annual performance, hourly wind speed and direction data are needed for a particular location. Modeling of hydro turbines needs hydrograph data which are listed on the United States Geological Survey website [52]. This data can help to design the micro-hydro turbines and predict their annual performance.

Hourly data obtained can be further used to calculate the amount of solar irradiation incident on the PV panels. The amount of incident irradiation also depends on the type of mounting system used for PV panels. Sun-tracking systems generally have higher incident energy compared with that on a fixed system planar system. Tracking systems can be classified as follows:

- Single axis tracking:
  - horizontal east–west,
  - horizontal north–south,
  - vertical.
- Two-axis tracking.

The amount of energy available to a variety of collector types and orientation has been developed for 239 physical locations in the US by the NREL [53]. In doing this, hourly data averaged over 30 years were used. Hourly data are available for simulation purposes. One comprehensive source is the TMY2 data [49].

Sun-tracking systems can enhance the collection yield significantly. When a large portion of the radiation is direct (compared with diffuse), concentrating systems can be used. The relation to calculate the amount on incident solar irradiation based on type of collector, whether tracking or not, is explained in a number of sources including the excellent text by Duffie and Beckman [54].

2.2. PV modeling

Photovoltaic cells are currently available in single and multi-junction forms. A problem inherent in photovoltaic devices is that they are able to interact only with a portion of the solar radiation distribution. Multi-junction cells are able to capture a wider portion of the

spectrum, and they show higher conversion efficiencies from sunlight-to-electricity than do single junction cells. Commonly available photovoltaic panels use single crystalline, polycrystalline, thin film or multi-junction cells. Many researchers have studied renewable hydrogen systems with photovoltaic cells (as mentioned in previous sections) as a source of energy for generating hydrogen.

Modeling PV arrays for renewable hydrogen systems can be accomplished by using the single diode model with equivalent circuit given in Fig. 2 [54]. This model uses the data provided by manufacturers (I_{sc}, U_{oc}, I_{mp}, U_{mp}, μ_{Isc}, and μ_{Uoc}) to model the PV performance.

The IV curve is calculated as a function of incident solar irradiation and cell temperature using Eq. (1) as follows:

$$I_{pv} = I_L - I_O\left[\exp\left[\frac{U_{pv} + I_{pv}R_s}{a}\right] - 1\right] - \frac{U_{pv} + I_{pv}R_s}{R_{sh}} \tag{1}$$

where light current (I_L), diode reverse saturation current (I_O), series resistance (R_s), shunt resistant (R_{sh}), and the parameter a are the five characteristics that are needed to solve Eq. (1). Based on the data from manufacturers, Eqs. (2)–(7) are solved simultaneously to obtain the reference values:

At the short circuit condition, $I_{pv} = I_{sc}$ and $U_{pv} = 0$,

$$I_{sc,ref} = I_{L,ref} - I_{O,ref}\left[\exp\left[\frac{I_{sc,ref}R_{s,ref}}{a_{ref}}\right] - 1\right] - \frac{I_{sc,ref}R_{s,ref}}{R_{sh,ref}} \tag{2}$$

At the open-circuit condition, $I_{pv} = 0$ and $U_{pv} = U_{oc}$,

$$0 = I_{L,ref} - I_{O,ref}\left[\exp\left[\frac{U_{oc,ref}}{a_{ref}}\right] - 1\right] - \frac{U_{oc,ref}}{R_{sh,ref}}. \tag{3}$$

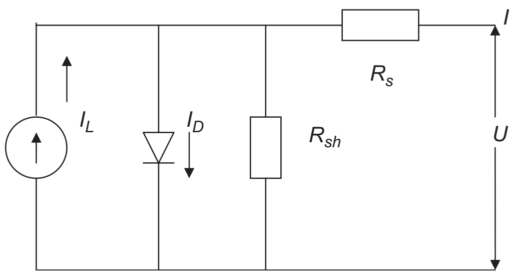


Fig. 2. The single diode equivalent circuit model.

At the maximum power point,

$$I_m = I_{L,ref} - I_{O,ref}\left[\exp\left[\frac{U_m + I_m R_{s,ref}}{a_{ref}}\right] - 1\right] - \frac{U_m + I_m R_{s,ref}}{R_{sh,ref}}. \tag{4}$$

Also at maximum power point,

$$\left.\frac{\mathrm{d}P_{pv}}{\mathrm{d}U_{pv}}\right|_m = 0 = I_m + U_m \left.\frac{\mathrm{d}I_{pv}}{\mathrm{d}U_{pv}}\right|_m, \tag{5}$$

where

$$\left.\frac{\mathrm{d}I_{pv}}{\mathrm{d}U_{pv}}\right|_m = \frac{-\frac{I_{O,ref}}{a_{ref}}\exp\left[\frac{U_{m,ref}+I_{m,ref}R_{s,ref}}{a_{ref}}\right] - \frac{1}{R_{sh,ref}}}{1 + \left(\frac{I_{O,ref}R_{s,ref}}{a_{ref}}\right)\exp\left[\frac{U_{m,ref}+I_{m,ref}R_{s,ref}}{a_{ref}}\right] + \frac{R_{s,ref}}{R_{sh,ref}}}. \tag{6}$$

And, checking the condition for estimation of the open-circuit voltage predicted by model, it is given as

$$\frac{\partial U_{oc}}{\partial T} = \mu_{U_{oc}} \approx \frac{U_{oc}(T_{pv}) - U_{oc}(T_{pv,ref})}{T_{pv} - T_{pv,ref}}. \tag{7}$$

The reference values are used to calculate the five parameters at operating condition using Eqs. (8)–(13):

$$a = a_{ref}\frac{T_{pv}}{T_{pv_{ref}}}, \tag{8}$$

$$I_L = \frac{S_{pv}}{S_{pv,ref}}[I_{L_{ref}} + \mu_{I_{sc}}(T_{pv} - T_{pv_{ref}})], \tag{9}$$

$$I_o = I_{o_{ref}}\left(\frac{T_{pv}}{T_{pv_{ref}}}\right)^3 \exp\left[\left.\frac{E_g}{kT}\right|_{T_{c_{ref}}} - \left.\frac{E_g}{kT}\right|_{T_c}\right]. \tag{10}$$

Here,

$$E_g = E_{g_{ref}}[1 - C(T_{pv} - T_{pv,ref})], \tag{11}$$

$$R_{sh} = R_{sh_{ref}}\frac{S_{pv,ref}}{S_{pv}}, \tag{12}$$

$$R_s = R_{s_{ref}}. \tag{13}$$

Finally, using the 5 parameters at the operating conditions, we can either calculate the current at a given voltage or use (14) and (15) for calculating current and voltage at maximum power point:

$$I_m = I_L - I_o\left[\exp\left[\frac{U_m + I_m R_s}{a}\right] - 1\right] - \frac{U_m + I_m R_s}{R_{sh}}, \tag{14}$$

$$0 = I_m + U_m \left[\frac{-\frac{I_O}{a}\exp\left[\frac{U_m+I_mR_s}{a}\right] - \frac{1}{R_{sh}}}{1 + \frac{I_OR_s}{a}\exp\left[\frac{U_m+I_mR_s}{a}\right] + \frac{R_s}{R_{sh}}} \right]. \tag{15}$$

Performance of the PV cell is very much dependent on the cell temperature which itself is a function of solar irradiation, ambient temperature, wind speed, wind direction type of mounting, and other factors. An energy balance for the PV cells can be used to find the cell temperature from Eq. (16) [54]:

$$\frac{T_{pv} - T_a}{T_{NOCT} - T_{a,NOCT}} = \frac{G_T}{G_{NOCT}} \frac{U_{L,NOCT}}{U_L} \left[1 - \frac{\eta_{c,pv}}{(\tau\alpha)}\right], \tag{16}$$

where

$$\eta_{c,pv} = \frac{I_m U_m}{A_{pv} G_T}. \tag{17}$$

Eq. (16) can be solved in an iterative way to obtain the cell temperature. The cell temperature can also be solved as an explicit function of incident solar irradiation, ambient temperature, and wind speed using Eqs. (18) and (19) [55]:

$$T_{pv} = T_{m,pv} + \frac{G_T}{G_{NOCT}} \Delta T_{pv}, \tag{18}$$

where T_m is the back surface temperature of module and is given by

$$T_{m,pv} = T_a + G_T e^{(a_c + b_c WS)}. \tag{19}$$

Figs. 3–6 show the performance of PV panels of 65 W rating. The data available from the manufacturer are $I_{sc} = 4.5\,V$, $U_{oc} = 21.4$, $I_m = 3.95$, $U_m 16.5$, $\mu_{Isc} = 0.00026$, $\mu_{Uoc} = -0.85$, $A_{pv} = 0.633$, and $Ns = 36$, as reported in [54]. Using the 5-parameter model noted above, the performance of the PV panels has been calculated. Fig. 3 indicates the *I–U* curves at different levels of solar irradiation at a cell temperature 40 °C. The maximum power point curve is also shown in Fig. 3. *I–U* curve and the power vs. *U* curves

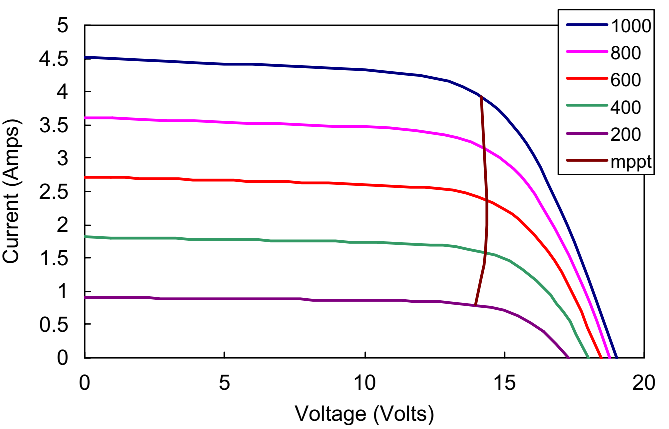


Fig. 3. *I–U* curve and maximum power point curve for different incident solar irradiation (W/m^2) at 40 °C for a PV panel.

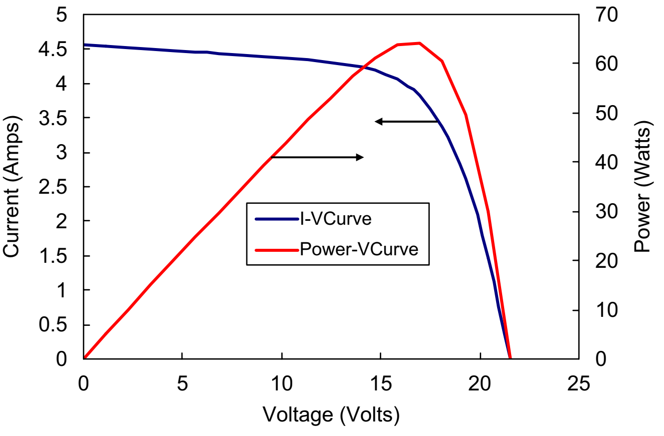


Fig. 4. I–U curve and power vs. U curve for a PV panel at 1000 W/m^2 solar irradiation and 25 °C temperature.

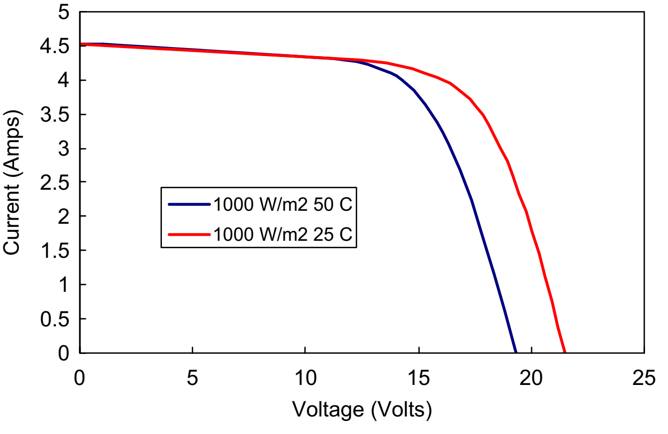


Fig. 5. The effect of temperature on the performance of a PV panel.

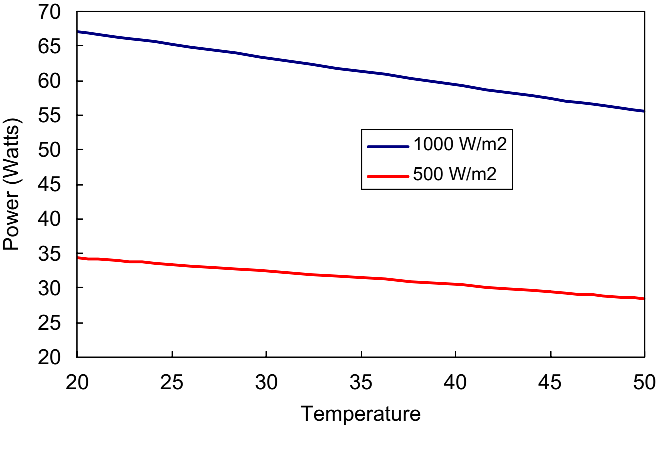


Fig. 6. Effect of temperature on maximum power of a PV panel.

Table 1
Values of empirical constants a_c, b_c, and ΔT_{pv} for various types of PV panels and mounting arrangements [55]

Module parameters	Module	a_c	b_c	ΔT_{pv} (°C)
Glass/cell/glass	Open rack	−3.47	−0.0594	3
Glass/cell/glass	Close roof mount	−2.98	−0.0471	1
Glass/cell/polymer sheet	Open rack	−3.56	−0.075	3
Glass/cell/polymer sheet	Insulated back	−2.81	−0.0455	0
Polymer/thin film/steel	Open rack	−3.58	−0.113	3
22X linear concentrator	Tracker	−3.23	−0.13	13

are shown in Fig. 4 at a solar irradiation of 1000 W/m^2 and cell temperature of 25 °C. The effect of temperature on the I–U characteristics of the PV panel is depicted in Fig. 5. The effect of temperature on the maximum power point for different levels of solar irradiation is shown in Fig. 6. It can be observed that performance changes significantly as the cell temperature changes. It is crucial to develop the methods to keep the cell temperature as low as possible to improve the performance of the PV cells (Table 1).

Other formulations for modeling photovoltaic devices have been reported. For example, King [55,56] and Luft et al. [57] have given examples of this. King et al. [55,56] developed an empirical model for simulating the performance of various PV technologies (the models take electrical, thermal, solar spectral and optical effects into consideration).

Empirical parameters found were specific for each type of module and a list of these is maintained at Sandia National Laboratories website [58]. Luft et al. [57] developed a model for predicting the current produced based on the I_{sc}, I_m, U_m, U_{oc}. Hadj et al. [59] developed different relations to evaluate the five parameters used in Eq. (1) for modeling PV performance. Comparisons of these models for representing PV performance are given in [60].

2.3. Wind machine modeling

Studies of combined PV and wind power have been reported [26,29,35,36,40–42,44]. Modeling was generally based on the machine performance data available from the manufacturer. Fig. 7 shows the experimental and calculated (using (21)) wind speed vs. power generated for a 2.5 kW rated wind turbine [61]. With the wind data for a location known, the amount of power generated can be estimated over a year's period.

Theoretical available wind power for a particular location can be calculated using

$$P_{th,wt} = \tfrac{1}{2}\rho_{air}A_{wt}^2\,WS^3. \tag{20}$$

The power in the wind must be modified by the "fractional efficiency" to determine the power out of the wind machine. Typical values of this parameter will be in the range 0.15–0.30.

A polynomial fit can be obtained to obtain power as a function of wind speed for any location and a particular wind turbine. The result for the data shown in Fig. 7 is as given in Eq. (21):

$$P_{a,wt} = -0.177\,WS^4 + 3.164\,WS^3 + 6.757\,WS^2 - 25.042\,WS + 2.119. \tag{21}$$

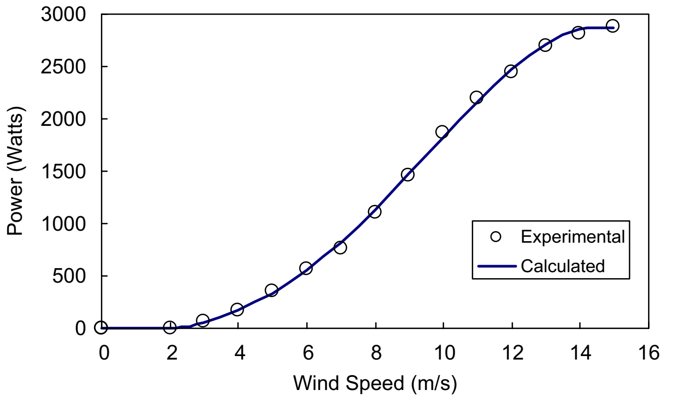


Fig. 7. An example trace of power output for a range of wind speeds is shown (after [61]).

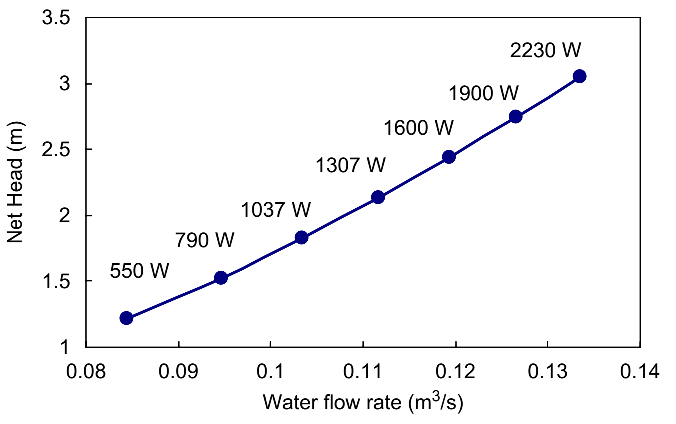


Fig. 8. Maximum power generated for a particular hydro turbine is shown as a function of water flow rate and net head [62].

2.4. Micro-hydro turbine modeling

Studies of micro-hydro turbine powering hydrogen generation have been reported [36,37,39]. The modeling was done based on the data available from the manufacturers of the equipment used. Generally for residential applications, low head hydro turbines (e.g., reaction turbines) can be used. An example of data available from a manufacturer for a reaction turbine with rated power 2.2 kW [62] is shown in Fig. 8.

Actual power generated for the hydro-turbine as a function of head and flow rate can be calculated using Eq. (22). Note that power generated is a linear function of flow rate and head available. The efficiency for the turbine given is approximately

$$P_{a,ht} = \eta \rho g Q h. \tag{22}$$

2.5. Electrolyzer modeling

Electrolyzers are devices that use electricity to split water into hydrogen and oxygen. The semi-empirical model of an alkaline electrolyzer was reported in [63,64]. The reactions at the anode and cathode of the electrolyzer cell are given as follows:

$$\text{Anode}: \; H_2O = 2H^+ + \tfrac{1}{2}O_2 + 2e^-. \tag{23}$$

$$\text{Cathode}: \; 2H^+ + 2e^- = H_2. \tag{24}$$

The semi-empirical model described in [63] could be easily applicable to PEM electrolyzers with a change in the empirical constants. The voltage required for the electrolyzer is obtained from the summation of the reversible voltage and summation of losses due to various resistances in the cell. The losses can be classified as activation losses, which quantify for slow electro-kinetics, ohmic losses in the cell and the concentration losses, which occur at higher current densities due to improper mass transfer of the species:

$$U_{el} = U_{rev} + \eta_{act} + \eta_{ohm} + \eta_{conc}. \tag{25}$$

Reversible voltage as a function of temperature and pressure can be given from the Nernst equation [64] as follows:

$$U_{rev} = \frac{1}{nF}\left[U_0 + RT\ln\left[p_{H_2}p_{O_2}^{1/2}\right]\right], \tag{26}$$

where U_0 is the standard cell potential and is calculated from the standard Gibbs free energy using Eq. (27). For the case of an electrolyzer reaction, the Gibbs free energy change is a positive quantity, and at standard conditions (25 °C and 1 bar) it is equal to 237.13 kJ/mol:

$$U_0 = \frac{\Delta G}{nF}. \tag{27}$$

The Gibbs free energy is a function of temperature and pressure. It can be obtained from a change in the enthalpy of formation and a change in entropy using Eq. (28). The change in enthalpy of formation and entropy as functions of temperature and pressure can be first obtained for individual species from Eqs. (31) and (32) [65]. Then the other parameters can be evaluated for the electrolyzer cell using Eqs. (29) and (30):

$$\Delta G = \Delta H - T\Delta S, \tag{28}$$

$$\Delta H = \Delta H_{H_2} + \tfrac{1}{2}\Delta H_{O_2} - \Delta H_{H_2O}, \tag{29}$$

$$\Delta S = \Delta S_{H_2} + \tfrac{1}{2}\Delta S_{O_2} - \Delta S_{H_2O}, \tag{30}$$

$$\Delta H = \Delta H^O + \int_{T_{ref}}^{T} Cp\,\mathrm{d}T, \tag{31}$$

$$\Delta S = \Delta S^O + \int_{T_{ref}}^{T} \frac{Cp}{T}\,\mathrm{d}T - R\ln\left(\frac{p}{p_{ref}}\right). \tag{32}$$

The specific heat at constant pressure can be expressed as a function of temperature using Eq. (33) [66]. Constants α, β, γ, δ, and ε can be obtained from Table 2. This function

Table 2
Constants for calculating specific heat at constant pressure, Eq. (33) [66]

Gas	α	$\beta \times 10^3$	$\gamma \times 10^6$	$\delta \times 10^9$	$\varepsilon \times 10^{12}$
H_2O	4.070	−1.108	4.152	−2.964	0.807
O_2	3.626	−1.878	7.055	−6.764	2.156
H_2	3.057	2.677	−5.810	5.521	−1.812

can be integrated and further used to evaluate changes in enthalpy and entropy of individual species using Eqs. (34) and (35):

$$C_p = R\left[\alpha + \beta T + \gamma T^2 + \delta T^3 + \varepsilon T^4\right], \tag{33}$$

$$\Delta H = \Delta H^O + R\left(\alpha T + \frac{\beta T^2}{2} + \frac{\gamma T^3}{3} + \frac{\delta T^4}{4} + \frac{\varepsilon T^5}{5}\right), \tag{34}$$

$$\Delta S = \Delta S^O + R\left(\alpha \ln T + \beta T + \frac{\gamma T^2}{2} + \frac{\delta T^3}{3} + \frac{\varepsilon T^4}{4}\right) - R \ln\left(\frac{p}{p_{ref}}\right). \tag{35}$$

The reversible potential U_{rev} can be easily determined from Eq. (26) as a function of temperature and pressure. Following that, the electrolyzer cell potential can be evaluated from Eq. (36). Note that the empirical parameters r, s, and t can be obtained by curve-fitting manufacturers' data. The second term on the right-hand side quantifies the ohmic resistance:

$$U_{el} = U_{rev} + \frac{r}{A} I_{el} + s \log\left(\frac{t}{A} I_{el} + 1\right), \tag{36}$$

where the empirical parameters r and t can be defined as function of operating temperature using Eqs. (37) and (38). Note that the temperature is in Celsius units for calculating r and t:

$$r = r_1 + r_2 \frac{T}{T_{ref}}, \tag{37}$$

$$t = t_1 + t_2 \frac{T_{ref}}{T} + t_3 \frac{T_{ref}^2}{T^2}. \tag{38}$$

The amount of hydrogen produced is given by

$$\dot{n}_{H_2} = \eta_F \frac{N_{c,el} I_{el}}{nF}, \tag{39}$$

where η_F is the Faraday efficiency which is the ratio of actual hydrogen produced to theoretical maximum possible production. Similarly, the amount of water required for a specific amount of hydrogen production and the corresponding amount of oxygen

produced are given by

$$\dot{n}_{H_2O} = \dot{n}_{H_2} = 2\dot{n}_{O_2}. \tag{40}$$

Performance of the electrolyzer is dependent on the operating temperature. The temperature can be either assumed constant or can be calculated by using a thermal model. A lumped thermal capacitance model [63] can be used to predict the temperature of the electrolyzer:

$$C_t \frac{\mathrm{d}T}{\mathrm{d}t} = Q_{gen} - Q_{loss} - Q_{cool}, \tag{41}$$

where Q_{gen} is the internal heat generation of the electrolyzer, Q_{loss} the heat lost to the ambient, and Q_{cool} the amount of cooling required to keep the electrolyzer at a rated condition. These are given as follows:

$$Q_{gen} = N_{c,el}(U_{el} - U_{tn})I_{el}, \tag{42}$$

where

$$U_{tn} = \frac{\Delta H}{nF}, \tag{43}$$

$$Q_{loss} = \frac{1}{R_{t,el}}(T - T_a). \tag{44}$$

A common method of cooling an electrolyzer is to flow excess water through the unit as compared with the water required for the actual hydrogen consumption. In this case, it can be assumed that the water flow related to the cooling requirement is

$$Q_{cool} = C_{cw}(T_{cw,i} - T_{cw,o}) = UA_{hx}\,LMTD. \tag{45}$$

It is worth mentioning that there is a paucity of publications related to studies of electrolyzers. More data are required to model the electrolyzer properly based on the physical behavior. It is imperative to provide a good basis for the semi-empirical parameters used in the model for calculating I– V curve, thermal model, etc.

Using the above approach, the effect of temperature and pressure on the I–V curves of the PEM electrolyzer is plotted. In the report by Cropley [67], experimental data were available for only one temperature and one pressure. Using this data, the empirical constants were obtained for the best fit and the effect for different temperature and pressures were calculated. See Figs. 9 and 10.

Some recent studies have focused on the search for improved and cheaper catalyst alternatives for hydrogen and oxygen evolution. The performance of cobalt and nickel glyomines is found to be inferior as compared with platinum for hydrogen evolution at cathode [68]. Authors reported the performance of Ir/Sn, Ir/Ru-based oxides for oxygen evolution at the anode. An efficiency of 94.4% for a single cell PEM electrolyzer was achieved with Ir/Ru at anode and Pt/C catalyst at cathode. Ir/Sn was not found to be effective catalyst for oxygen evolution [69,70].

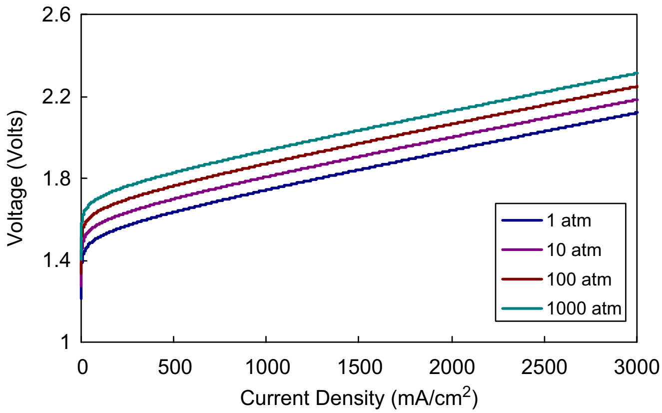


Fig. 9. Effect of operating pressure on the performance of an electrolyzer cell.

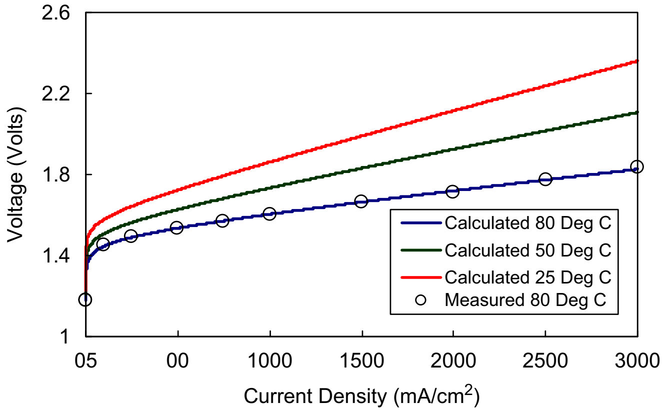


Fig. 10. Effect of temperature on the performance of an electrolyzer cell.

2.6. Fuel cell modeling

A fuel cell is an electrochemical device that converts hydrogen and oxygen gas into electrical current (DC). A review of fuel cell modeling based on analytical, semi-empirical, and mechanistic approaches has been given by Cheddie and Munroe [71]. Modeling of fuel cells for system analysis purposes was initially proposed by Vanhanen et al. [32], Chamberlin [72], Lee [73], and Amphett [74]. Further improvement in the fuel cell model of Amphett et al. was reported in [75–79].

The reactions at the anode and cathode are given as follows:

$$\text{Anode}:\ H_2 = 2H^+ + 2e^-. \tag{46}$$

$$\text{Cathode}:\ 2H^+ + \tfrac{1}{2}O_2 + 2e^- = H_2O. \tag{47}$$

Electrical energy, water, and heat are the three products of this reaction. The total cell potential can be obtained from

$$U_{fc} = U_{rev} + \eta_{act} + \eta_{conc} + \eta_{ohm}. \tag{48}$$

where U_{rev} is the reversible voltage as a function of temperature and pressure can be obtained from the Nernst equation [65]. The first term gives the variation of standard potential of the fuel cell with respect to temperature and pressure:

$$U_{rev} = \frac{1}{nF}\left[U_{0,fc} + RT\,\ln\left(p_{H_2}p_{O_2}^{1/2}\right)\right]. \tag{49}$$

$U_{0,fc}$ is the standard cell potential of the cell. It can be calculated as a function of temperature and pressure from the relations developed for electrolyzers. The only difference is that the products and reactants are opposite from that of an electrolyzer and are given by Eqs. (50) and (51):

$$\Delta H = \Delta H_{H_2O} - \Delta H_{H_2} - \tfrac{1}{2}\Delta H_{O_2}, \tag{50}$$

$$\Delta S = \Delta S_{H_2O} - \Delta S_{H_2} - \tfrac{1}{2}\Delta S_{O_2}. \tag{51}$$

Activation polarization η_{act} is the extra voltage applied to counteract the slow reaction rate at the electrodes of fuel cells. The reaction rate can be increased either by increasing the process gas flow rate and thereby increasing the process gas kinetic energy; or by adding extra voltage and thereby reducing the energy output of the fuel cell. According to Faraday's law, the reaction rate is proportional to the current density; and a lower reaction rate implies lower current densities. Other means of reducing the activation potential besides increasing the process gas flow rates include: increasing active area of the electrode, increasing operating temperature and increasing the utilization of catalyst [73].

The expression for the activation polarization (anode + cathode) was derived in [78,79] from Butler–Volmer equation as follows:

$$\eta_{act} = \xi_1 + \xi_2 T + \xi_3 T\,\ln(c^*_{O_2}) + \xi_4 T\,\ln(i), \tag{52}$$

where ξ_1, ξ_2, ξ_3, ξ_4 are given as follows:

$$\xi_1 = -\left[\frac{\Delta G_{ec}}{2F}\right] - \left[\frac{\Delta G_e}{\alpha_c n_c F}\right], \tag{53}$$

$$\xi_2 = \frac{R}{\alpha_c n_c F}\ln\left[nFk_c^0(c^*_{H^+})^{(1-\alpha_c)}(c^*_{H_2O})^{(\alpha_c)}(k_a^0)^{\frac{n\alpha_c}{2}}\right] + \left(\frac{R}{2F} + \frac{R}{\alpha_c n_c F}\right)\ln\left[A_{fc}\right] + \left(\frac{R}{2F}\right)\ln\left[4Fc^*_{H_2}\right], \tag{54}$$

$$\xi_3 = \frac{R}{\alpha_c nF}(1-\alpha_c), \tag{55}$$

$$\xi_4 = -\left(\frac{R}{\alpha_c n_c F} + \frac{R}{2F}\right). \tag{56}$$

Numerical values for the ξ_1, ξ_2, ξ_3, ξ_4 parameters were provided for a Ballard fuel cell [77,78] as follows:

$$\begin{aligned}
\xi_1 &= -0.948(\pm 0.004),\\
\xi_2 &= k_{DR}\frac{age}{T} + k^0_{cell} + 0.000197\ \ln(A_{fc}) + 4.3 \times 10^5\ \ln(c^*_{H_2}),\\
\xi_3 &= 6.8 \pm 0.02 \times 10^{-5},\\
\xi_4 &= -1.97 \pm 0.05 \times 10^{-4}.
\end{aligned}$$

These values could be changed within given limits for modeling PEM fuel cells from other manufacturers.

Ohmic polarization, η_{ohm}, is the extra voltage needed to overcome the electrical resistance offered by the cell to the electron and proton transfer within the cell. Note that the resistance to the electron transfer could be due to electrodes, graphite collector plates, and other fixtures that connect the membrane electrode assemblies (MEA) together. This resistance could be decreased by using materials that are good electrical conductors. Proton conductivity could be improved by reducing the thickness of the membrane. The ohmic polarization can be estimated as follows [78]:

$$\eta_{ohm} = -i(R^{electronic} + R^{proton}) = -iR^{internal}. \tag{57}$$

Here, $R^{electronic}$ includes resistance due to contact resistance. For pure graphite plates the actual $R^{electronic}$ should not be significant in comparison to R^{proton} [79]. R^{proton} can be obtained as follows:

$$R^{proton} = \frac{r_m L}{A_{fc}}, \tag{58}$$

where L and A_{fc} are the thickness and the area of the membrane, respectively, and r_m is the membrane specific resistivity for the proton transfer from the membrane. The latter is a function of the type and characteristics of the membrane, water content of membrane, temperature, and current density. For Nafion membranes the following relationship for r_m was proposed [78]:

$$r_m = \frac{181.6\left[1 + 0.03\left(\frac{i}{A_{fc}}\right) + 0.062\left(\frac{T}{303}\right)^2\left(\frac{i}{A_{fc}}\right)^{2.5}\right]}{\left[\lambda^0 + \lambda_{DR}\,age - 0.634 - 3\left(\frac{i}{A_{fc}}\right)\right]\exp\left(4.18\left[\frac{T-303}{T}\right]\right)}. \tag{59}$$

The voltage degradation effect on the performance of fuel cells was studied in [79]. Aging phenomena are introduced in the model through the λ terms in ohmic losses and k_{cell} in activation potential losses.

Concentration polarization η_{conc} is the extra voltage required to overcome the resistance to the mass transport of the process gases at the reaction sites on membrane electrode assembly. Mass transport includes the transport of gases to the reaction site (flow through channels and diffusion in the electrodes) and removal of water and other impurities from the reaction site. At the lower current densities, these losses are not significant as compared with higher current densities. At higher current densities, process gases should reach the reaction sites at higher rates and similarly the water and other impurities should be removed more quickly from the reaction sites. Concentration polarization can be estimated

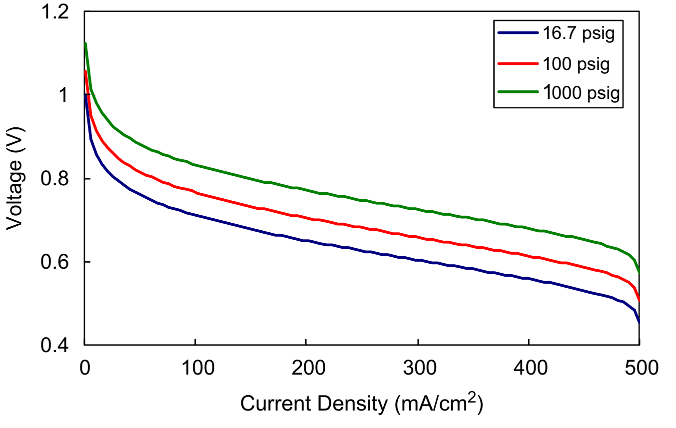


Fig. 11. Effect of pressure on the performance of the fuel cell.

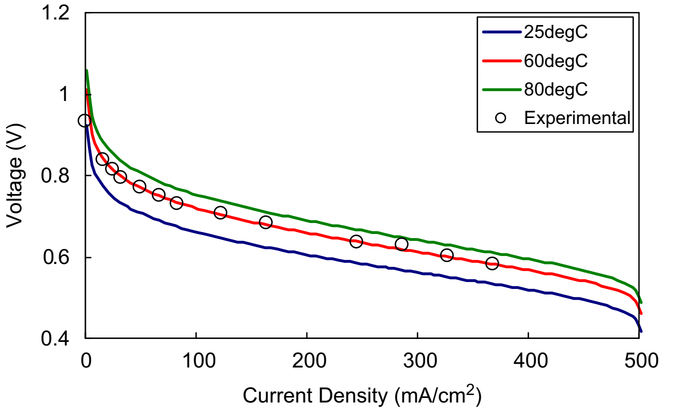


Fig. 12. Effect of temperature on the performance of a fuel cell.

as follows [80]:

$$\eta_{conc} = \frac{RT}{nF}\left[1 - \frac{i}{i_L}\right]. \tag{60}$$

Hence, the I–U curve of the PEM fuel cell can be obtained using Eq. (48) considering the losses due to activation, ohmic and concentration polarizations. Figs. 11 and 12 show the performance of the 1.4 kW fuel cell stack. The experimental data used for this purpose were reported on the web [81]. Figs. 11 and 12 show the effects of pressure and temperature on the performance of the fuel cell, respectively.

Similar to electrolyzers, a fuel cell's performance is also temperature dependent. In a manner similar to what is done relative to an electrolyzer a thermal model can be used for predicting the temperature of the fuel cell. Internal heat generation for this case would be as follows:

$$Q_{gen} = N_{c,fc}(U_{tn} - U_{fc})I. \tag{61}$$

In addition, a fuel cell's heat loss can be calculated using a heat balance across the inlet and outlet streams of hydrogen and oxygen flow. In the case of a hydrogen/air fuel cell, it must be remembered that the oxygen side balance involves 21% of the total atmospheric air flow. Some recent studies have focused on accurately predicting the activation and concentration polarization [82–84]. The evaluation of activation and concentration polarizations at the anode and the cathode is based on a function of the concentration and partial pressures of the reactant gases (H_2 and O_2) that are related to each other by Henry's law. Once the exchange current density is obtained, the approximations of Butler–Volmer relationship for lower and higher polarization can be used to obtain the activation potential for the anode and the cathode [83]. A literature review regarding the mechanisms of hydrogen oxidation reaction on different platinum electrodes and their effect on the exchange current density has been given by Mann et al. [84].

2.7. Storage modeling

Hydrogen storage is one of the important aspects of the path towards a hydrogen economy. As was noted in the early part of this paper, many of the renewable sources have energy outputs that are quite variable in time, so a means of storing the results of capturing the energy is critical. The following are the commonly used hydrogen storage technologies [85–88] currently under research:

1. Compressed hydrogen.
2. Liquid hydrogen.
3. Metal hydrides.
4. Carbon-based materials (fullerenes, carbon nanotubes, activated carbons).

Discussions for all these forms and their current status have been given [85,87]. In this section, we will focus on modeling aspects of these technologies.

2.7.1. Compressed hydrogen storage

Modeling of compressed hydrogen gas storage can be accomplished by assuming with little error that hydrogen is an ideal gas. The amount of work required to compress hydrogen to a required pressure can be obtained by considering a polytropic process for compressor. The actual work required can then be found using a compressor efficiency, information usually furnished by the compressor manufacturer, using Eq. (62):

$$P_{comp} = \frac{1}{\eta_{comp}} \frac{n_{poly}}{n_{poly} - 1} n_{gas} RT \left[1 - \left(\frac{p_{c,out}}{p_{c,in}} \right)^{(n_{poly}-1)/n_{poly}} \right]. \tag{62}$$

And pressure inside the storage tank can be obtained from

$$p_{st} = \frac{n_{st} RT}{V_{st}}. \tag{63}$$

2.7.2. Liquefied hydrogen

In general, it is not anticipated that this approach will be used for most stand-alone hydrogen systems. Although it is possible, it seems that the nature of a liquefaction

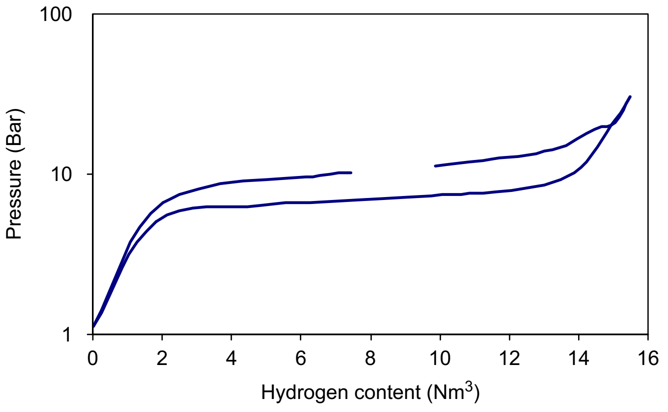


Fig. 13. Shown are the adsorption curve (upper curve) and desorption curve (lower curve) for a metal hydride hydrogen storage [11].

approach may be too complicated. Of course, the storage energy density is relatively high using a liquid compared with using even a very high-pressure gas. Good sources of information on this general topic are given in the literature [85,87,88].

2.7.3. Metal hydrides

Many metals and alloys have a tendency to combine with hydrogen to form hydrides [89]. When hydrogen is stored inside a hydride (also called as charging or hydriding), the heat is released during this filling operation. On the contrary, heat input is needed while taking hydrogen out from the hydride, also called discharging or dehydriding. This reversible process for metal M can be expressed as

$$M + 0.5xH_2 \Leftrightarrow MH_x + \text{heat}. \tag{64}$$

Including a metal hydride with the renewable hydrogen system needs a fairly simple model that includes the rate of hydrogen storage (includes hydriding and dehydriding), the amount of heat generated/required, as well as the operating temperature and pressure. Detailed modeling of the metal hydrides is reviewed in [85]. A database of metal hydrides and their properties is available on the web [90]. Using the lumped capacitance method the temperature of the bed as a function of time can be calculated [91] as well as the heat generated or required for hydriding or dehydriding. Based of bed temperature, the operating pressure can be found using Van Hoff's equation [85]:

$$C_{mh}\frac{\mathrm{d}T(t)}{\mathrm{d}t} = Q_{mh}(t) - k_{eff}[T(t) - T_a], \tag{65}$$

$$\ln(p_{eq}) = \frac{\Delta H}{RT} - \frac{\Delta S}{R}, \tag{66}$$

where Q_{mh} is a function of time because the heat would be released during the absorption and required during desorption. A basic assumption usually made in the modeling of hydride storage is that the cycling efficiency is 1, which means that there is no change in the adsorption and desorption properties of the MH. Fig. 13 shows the hydrogen adsorption and desorption curve at 5.3 °C for a MH bed of 19 N m^3 rated hydrogen storage capacity [11].

Metal hydride beds for hydrogen storage integrated with RHGUS have been reported in the literature [11,30,34]. Experimental data for the metal hydride bed integrated with an electrolyzer and a fuel cell were given by Vanhanen et al. [92].

2.7.4. Carbon-based materials for hydrogen storage

Carbon-based materials are capable of storing hydrogen. A review of work related to hydrogen storage in fullerenes, carbon nanotubes and activated carbons has appeared in the literature [86,93]. A wide range of hydrogen uptakes in carbon nanostructures has been reported [93].

Fullerenes are synthesized carbon molecules that resemble a football in shape. Experiments showing adsorption and desorption of hydrogen (up to 6 wt%) have been reported. The cyclic behavior of these materials is not impressive at this stage (as noted in [86]).

Two types of carbon nanotubes have been explored: single-wall nanotubes (SWNT) and multi-wall nanotubes. Hydrogen can be stored in carbon nanotubes by chemisorption or physisorption mechanisms. In chemisorption the hydrogen is covalently bonded with host materials. The desorption temperatures are too high ($>500\,K$). Physisorption occurs due to Van Der Waal's attractive forces between hydrogen and the host material (carbon) that stabilizes the hydrogen on the surface of carbon nanotubes. Desorption temperatures of hydrogen for SWNTs, in the vicinity of room temperature, have been reported [94].

Activated carbons demonstrate high surface areas and are able to adsorb hydrogen in bulk material micro-pores [86]. Experimental data reported by numerous researchers have been tabulated for hydrogen storage (wt%) in carbon nanotubes, carbon nanofibers—graphitic planes that are intercalated at a fixed distance (0.355) from each other—and activated carbons [93].

The effective integration of carbon nanostructure hydrogen storage with RHGUS or automobiles will require the development of this material with a capability of operating near ambient conditions ($25<T<100\,^{\circ}C$ and $P>1$ atm). Effective modeling tools must be developed to predict accurately the mechanisms of hydrogen storage in carbon nanostructures. The cyclic performance of carbon nanostructures needs to be addressed along with the degradation of performance with time.

2.8. Residential application

Energy consumption of a house can be generally categorized in two forms, electrical and thermal (as a fuel). The energy demand of any particular house is a direct function of the type of materials of construction and their ability to transfer heat from/to the surrounding atmosphere. It is crucial to have an energy efficient design for future residential houses because it will not only reduce the overall energy demand of the house but also be helpful to design economically feasible RHGUS configurations for this application.

The best possible scenario for designing RHGS/RHGUS for this application is to use actual energy demand data for the house on an annual basis. If this is not available, then the hourly electrical energy demand for the house can be obtained as given in what follows. Firstly, the cooling load and heating load demand can be estimated, as a function of design conditions and type of materials used, for the particular building [48]. The data for a

variety of structures and materials and their *R*-values (wall structure, roof, basement, doors, windows, lights, number of occupants, etc.) can be found using techniques summarized by ASHRAE [95]. Secondly, an overall heat transfer coefficient for the house, based on floor area, can be estimated for the design conditions of a particular location. This overall heat transfer coefficient can be further used to calculate the hourly electrical energy demand of the house as a function of ambient temperature. As an example, hourly energy demand for a standard house (1600 ft^2) located in Las Vegas, NV, has been reported [48].

Once the hourly electrical energy demand is known, the next step is to obtain the thermal energy demand. The hydrogen-based car as an example can currently go approximately an average of 56.5 miles/kg of hydrogen gas [96]. Assuming a certain percent of home refueling (0–100, where, 0 denotes the case with no hydrogen generated at home is used for fueling the car and 100 denotes all fuel needs of car are satisfied by hydrogen generated at home) can give the hydrogen required for driving the car. Besides this, the gas requirements for water heating, cooking, and drying can be estimated from data given by EERE [97]. Hourly residential gas requirements can be obtained by dividing the total amount of gas required by the number of hours in a year.

Recently, the potential for research to design energy efficient buildings has been reported. Numerous aspects of energy efficient design of walls, windows, lighting, etc. have been discussed [98]. Another study reported the evaluation of evaporative-water cooled air-conditioning systems as compared with conventional air-cooled systems for a house in a desert climate [99].

Based on these electrical and gas requirements a RHGS/RHGUS system can be designed and its performance can be predicted for a particular house for any location. Economic issues for a house system designed according to the information given above are not addressed here. However, it is worth mentioning that if the house is already grid connected, then the grid can be easily used as short-term storage as compared with a battery. Certainly, this would not be a case for an off-grid application.

3. Concluding assessment of state of system understanding

From this review, it can be concluded that a large amount of effort has been taken in the recent past to model the various components of RHGS/RHGUS, either based on individual components or collectively for the overall system. Because of this vast literature on simulation and experimental efforts the question that might be asked is ‘‘Do we have a good understanding of the methodology to model the individual components as well as the overall system associated with a RHGS/RHGUS?’’ This article is an attempt to explore details of an answer to this question. Although simulation information presented in this paper is chosen to reflect the proper physics involved with the major components, further research is needed to reduce/eliminate generally the empirical nature of the models.

The *input energy resources* needed for modeling purposes are well-quantified and over 30 years’ of data are readily available for many locations in US. *PV modeling* discussed here is well developed and can be applied to the different types of cells currently being manufactured. *Electrolyzer models* are less well developed. For example, the ones applicable to PEM technology are currently in crude form and need attention to include more of the nature of the physics involved. *Fuel cell modeling* has received several years of careful attention, and this area is fairly mature. Recently published papers illustrate that

general performance aspects of these devices can be predicted quite well. The physics for the description of *hydrogen storage of compressed gas* are well understood. Only simple simulation tools have been put forth for describing *metal hydride storage*; more data are needed on large-scale applications to model accurately this method of containing the gas. *Carbon-based storage technology* is in very early development stages so its ability to store effectively on large scale is still in question. On the other hand, *residential utilization* of hydrogen can be readily represented in simulations. The energy requirements for a house can be modeled easily using methodology that is well developed. However, the current designs of buildings that, in general, require large amounts of energy, will have to have large RHGUS installations, and these will be very expensive. More energy efficient design of buildings will open this market more quickly.

4. Recommendations for future work

Based on the conclusions, some of the key aspects from a modeling standpoint for the RHGS/RHGUS that needs to be addressed by the scientific community are listed below:

- Application of RHGS/RHGUS to homes is limited both by the relative immaturity of the technology, as well as the relatively large systems that would be needed. The development of standard designs of energy efficient residential houses is needed to reduce their energy demand. This will assist in decreasing the sizes of energy conversion equipment substantially. Appropriate methods to include the energy (electrical and thermal) efficient equipment and their effect on overall energy demands needs to be quantified.
- Simulation approaches to represent the performance of photovoltaic cells are well developed. Quantifying the degradation of performance with time for these devices needs to be addressed.
- Modeling insights for electrolyzers have to be improved significantly to show clearly the activation, ohmic and concentration polarization losses inside the cell. Since there is not enough data available for PEM electrolyzers, these aspects certainly should be addressed. Models need to be developed so that actual mechanisms of electrolysis can be reflected in it instead of theoretical estimates.
- CFD modeling has been widely used to simulate the multi-physical phenomena associated with fuel cells. Not nearly as much attention has been given to the PEM electrolyzers, and the understanding of this technology could gain a great deal from these types of efforts.
- Work related to the hydrogen storage technologies has been reported in [85]. The physics of some aspects of this important component of renewable systems are well understood, but there are several newer approaches that may hold great promise that need to be investigated further.
- The degradation of performance validated with actual experimental data needs to be addressed for almost all the components of RHGUS.
- Since the technology, manufacturing, and marketing of many of the RHGUS components are in early stages of development, costs of all the components of the RHGUS are very uncertain. This topic should be addressed now with prices estimated for the situation when this technology becomes more mature, and then revisited periodically as the market continues to grow.

Acknowledgments

The authors thank the US DOE for partial support related to projects in hydrogen system development.

References

[1] Eisenstadt MM, Cox KE. Hydrogen production from solar energy. Sol Energy 1975;17:59–65.
[2] Costogue EN, Yasui RK. Performance data for a terrestrial solar photovoltaic/water electrolysis experiment. Sol Energy 1977;19:205–10.
[3] Fischer M. Review of hydrogen production with photovoltaic electrolysis systems. Int J Hydrogen Energy 1986;11(8):495–501.
[4] Goswami DY, Mirabal ST, Goel N, Ingley HA. A review of hydrogen production technologies. First international conference on fuel cell science. Eng Technol 2003:61–74.
[5] Esteve D, Ganibal C, Steinmetz D, Vialaron A. Performance of a photovoltaic electrolysis system. Int J Hydrogen Energy 1982;7(9):711–6.
[6] Koukouvinos A, Lygerou V, Koumoutsos N. Design of a system for solar energy storage via water electrolysis. Int J Hydrogen Energy 1982;7(8):645–50.
[7] Dini D. Hydrogen production through solar energy water electrolysis. Int J Hydrogen Energy 1983; 8(11/12):897–903.
[8] Morimoto Y, Hayashi T, Maeda Y. Mobile solar energy hydrogen generating system. 21st Intersociety energy conversion engineering conference: advancing toward technology breakout in energy conversion; 1986. p. 1281–4.
[9] Kharkhats YI, German ED, Kazarinov VE, Pshenichnikov AG, Pleskov YV. Hydrogen production by solar energy: optimization of the plant "solar array + electrolyzer". Int J Hydrogen Energy 1986;11(10):617–21.
[10] Steeb H, Mehrmann A, Seeger W, Schnurnberger W. Solar hydrogen production: photovoltaic/electrolyzer system with active power conditioning. Int J Hydrogen Energy 1985;10(6):353–8.
[11] Hollmuller P, Joubert JM, Lachal B, Yvon K. Evaluation of a 5 kWp photovoltaic hydrogen production and storage installation for a residential home in Switzerland. Int J Hydrogen Energy 2000;25:97–109.
[12] Carpetis C. A study of water electrolysis with photovoltaic solar energy conversion. Int J Hydrogen Energy 1983;7(4):897–903.
[13] Leigh RW, Metz PD, Michalek K. Photovoltaic-electrolyzer system transient simulation results. J Solar Energy Eng 1986;108:89–94.
[14] Hancock Jr OG. A photovoltaic-powered water electrolyzer: its performance and economics. Int J Hydrogen Energy 1986;11(3):153–60.
[15] Seigel A, Schott T. Optimization of photovoltaic hydrogen production. Int J Hydrogen Energy 1988;13(11):659–75.
[16] Carpetis C. Break-even and optimization conditions for overall energy systems wherein hydrogen facilities are used. Int J Hydrogen Energy 1985;10(12):839–50.
[17] Bilgen E, Bilgen C. An assessment of large-scale solar hydrogen production in Canada. Int J Hydrogen Energy 1983;8(6):441–51.
[18] Vidueiraa JM, Contreras A, Veziroglu TN. PV autonomous installation to produce hydrogen via electrolysis, and its use in FC buses. Int J Hydrogen Energy 2003;28:927–37.
[19] Bilgen E. Domestic hydrogen production using renewable energy. Sol Energy 2004;77:47–55.
[20] Bilgen E. Solar hydrogen from photovoltaic-electrolyzer systems. Energy Convers Manage 2001;42:1047–57.
[21] Tani T, Sekiguchi M, Sakai M, Ohta D. Optimization of solar hydrogen systems based on hydrogen production cost. Sol Energy 2000;68(2):143–9.
[22] Park M, Lee DH, Yu IK. PSCAD/EMTDC modeling and simulation of solar-powered hydrogen production system. Renew Energy 2006;31:2342–55.
[23] Lehman PA, Chamberlin CE. Design of a photovoltaic-hydrogen-fuel cell energy system. Int J Hydrogen Energy 1991;16(5):349–52.
[24] Barra L, Coiante D. Hydrogen-photovoltaic stand-alone power stations: a sizing method. Int J Hydrogen Energy 1993;18(4):337–44.
[25] Szyszka A. Ten years of solar hydrogen demonstration project at Neunburg Vorm Wald, Germany. Int J Hydrogen Energy 1998;23(10):849–60.

[26] Ghosh PC, Emonts B, Stolten D. Ten years of operational experience with a hydrogen-based renewable energy supply system. Sol Energy 2003;75:469–78.
[27] Goetzberger A, Bopp G, Griebhaber W, Stahl W. The PV/hydrogen/oxygen system of the self-sufficient solar house Frieburg. IEEE 1993:1152–8.
[28] Lehman PA, Chamberlin CE, Pauletto G, Rocheleau MA. Operating experience with a photovoltaic-hydrogen energy system. Int J Hydrogen Energy 1997;22(5):465–70.
[29] Agbossou K, Chahine R, Hamelin J, Laurencelle F, Anouar A, St-Arnaud JM, et al. Renewable energy systems based on hydrogen for remote applications. J Power Sources 2001;96:168–72.
[30] Chaparro AM, Soler J, Escudero MJ, De Ceballos EML, Wittstadt U, Daza L. Data results and operational experience with a solar hydrogen system. J Power Sources 2005;144:165–9.
[31] Tani T, Iwaki T, Suzuki H. Fundamental study on hydrogen production by photovoltaic power systems. ASME-JSES-KSES International Solar Energy Conference Part 1 (of 2); 1992. p. 517–21.
[32] Vanhanen JP, Kauranen PS, Lund PD, Manninen LM. Simulation of solar hydrogen energy systems. Sol Energy 1994;53(3):267–78.
[33] Ulleberg $\varnothing$, Morner SO. TRNSYS simulation models for solar-hydrogen systems. Sol Energy 1997;59(4–6):271–9.
[34] Vosen SR, Keller JO. Hybrid energy storage systems for stand-alone electric power systems: optimization of system performance and cost through control strategies. Int J Hydrogen Energy 1999;24(12): 1139–56.
[35] Kolhe M, Agbossou K, Hamelin J, Bose TK. Analytical model for predicting the performance of photovoltaic array coupled with a wind turbine in a stand-alone renewable energy system based on hydrogen. Renew Energy 2003;28(5):727–42.
[36] Santrelli M, Cali M, Macagno S. Design and analysis of stand-alone hydrogen energy systems with different renewable sources. Int J Hydrogen Energy 2004;29(15):1571–86.
[37] Santarelli M, Macagno S. Hydrogen as an energy carrier in stand-alone applications based on PV and PV-micro-hydro systems. Energy 2004;29:1159–82.
[38] Santarelli M, Macagno S. A thermoeconomic analysis of a PV-hydrogen system feeding the energy requests of a residential building in an isolated valley of the Alps. Energy Convers Manage 2004;45(3):427–51.
[39] Santarelli M, Pellegrino D. Mathematical optimization of a RES-H2 plant using a black box algorithm. Renew Energy 2005;30(4):493–510.
[40] Agbossou K, Kolhe M, Hamelin J, Bose TK. Performance of stand-alone renewable energy system based on energy storage as hydrogen. IEEE Trans Energy Convers 2004;19(3):633–40.
[41] Abbossou K, Kolhe ML, Hamelin J, Bernier E, Bose TK. Electrolytic hydrogen based renewable energy system with oxygen recovery and re-utilization. Renew Energy 2004;29(8):1305–18.
[42] Kélouwani S, Agbossou K, Chahine R. Model for energy conversion in renewable energy system with hydrogen storage. J Power Sources 2005;140:392–9.
[43] Ulleberg O. The importance of control strategies in PV-hydrogen systems. Sol Energy 2004;76:323–9.
[44] Mills A, Al-Hallaj S. Simulation of hydrogen-based hybrid systems using Hybrid2. Int J Hydrogen Energy 2004;29(10):991–9.
[45] Hedström L, Wallmark C, Alvfors P, Rissanen M, Stridh B, Ekman J. Description and modeling of the solar-hydrogen-biogas-fuel cell system in GlashusEtt. J Power Sources 2004;131:340–50.
[46] Shapiro D, Duffy J, Kimble M, Pien M. Solar powered regenerative PEM electrolyzer/fuel cell system. Sol Energy 2005;79:544–50.
[47] Maclay JD, Brouwer J, Samuelsen GS. Dynamic analysis of regenerative fuel cell power for potential use in renewable residential applications. Int J Hydrogen Energy 2006;31:994–1009.
[48] Deshmukh SS, Boehm RF. Mathematical modeling of performance of a grid-connected solar-hydrogen system for residential applications. J Energy Climate Change 2006;1(2):113–24.
[49] http://rredc.nrel.gov/solar/old_data/nsrdb/hourly/.
[50] http://rredc.nrel.gov/wind/pubs/atlas/.
[51] ftp://ftp.wcc.nrcs.usda.gov/downloads/climate/windrose.
[52] http://www.geology.sdsu.edu/classes/geol351/hydrographs.htm.
[53] Marion W, Wilcox S. Solar radiation data manual for flat plate and concentrating collectors. NREL; 1994.
[54] Duffie JA, Beckman WA. Solar engineering of thermal processes. 3rd ed. New York: Wiley, Inc.; 2006.

[55] King DL, Boyson WE, Krotochvil JA. Photovoltaic array performance model. SAND2004-3535, August 2004.
[56] King DL, Kratochvil JA, Boyson WE, Bower WI. Field experience with a new performance characterization procedure for photovoltaic arrays. In: Second world conference and exhibition on photovoltaic solar energy conversion, Vienna, Austria 1998.
[57] Luft W, Barton JR, Conn AA. Multifaceted solar array performance determination. TRW Systems Group, Redondo Beach, California, February 1967.
[58] http://www.sandia.gov/pv/docs/Database.htm.
[59] Hadj Arab A, Chenlo F, Benghanem M. Loss-of-load probability of photovoltaic water pumping systems. Sol Energy 2004;76:713–23.
[60] De Soto W. Improvement and validation of a model for photovoltaic array performance. MS thesis, Mechanical Engineering, University of Wisconsin-Madison, 2004.
[61] http://www.solarwindworks.com/Products/Wind_Turbines/Proven/Proven_Specs/proven_specs.htm.
[62] http://www.absak.com/pdf/neptunespec.pdf.
[63] Ulleberg Ø. Modeling of advanced electrolyzers: a system simulation approach. Int J Hydrogen Energy 2003;28:21–33.
[64] Hug W, Bussmann H, Brinner A. Intermittent operation and operation modeling of an alkaline electrolyzer. Int J Hydrogen Energy 1993;18:973–7.
[65] Atkins P. Physical chemistry. 6th ed. New York: W.H. Freeman and Company; 1997.
[66] Moran MJ, Shapiro HN. Fundamentals of engineering thermodynamics. 5th ed. New York: Wiley, Inc.; 2004.
[67] Cropley C. Low-cost, high-pressure hydrogen generator. DOE Hydrogen Program Review; 2005.
[68] Patani O, Anxolabéhère-Mallart E, Aukauloo A, Millet P. Electroactivity of cobalt and nickel glyxomines with regard to the electro-reduction of protons into molecular hydrogen in acidic media. Electrochem Commun 2007;9:54–8.
[69] Marshall A, Børessem B, Hagen G, Tsypkin M, Tunold R. Electrochemical characterization of $Ir_xSn_{1-x}O_2$ powders as oxygen evolution electrocatalysts. Electrochim Acta 2006;51:3161–7.
[70] Marshall A, Børessem B, Hagen G, Tsypkin M, Tunold R. Hydrogen production by advanced proton exchange membrane (PEM) water electrolyzers-reduced energy consumption by improved electrocatalysis. Energy 2007;32:431–6.
[71] Cheddie D, Munroe N. Review and comparison of approaches to proton exchange membrane fuel cell modeling. J Power Sources 2005;147:72–84.
[72] Kim J, Lee SM, Srinivasan S, Chamberlin CE. Modeling of proton exchange membrane fuel cell performance with an empirical equation. J Electrochem Soc 1995;142(8):2670–4.
[73] Lee JH, Lalk TR, Appleby AJ. Modeling electrochemical performance in large scale proton exchange membrane fuel cell stacks. J Power Sources 1998;70:258–68.
[74] Amphlett JC, Baumert RM, Mann RF, Peppley BA, Roberge PR, Rodrigues A. Parametric modeling of the performance of a 5 kW proton-exchange membrane fuel cell stack. J Power Sources 1994;49:349–56.
[75] Amphlett JC, Baumert RM, Mann RF, Peppley BA, Roberge PR, Harris TJ. Performance modeling of the Ballard Mark IV solid polymer electrolyte fuel cell (I. Mechanistic model development). J Electrochem Soc 1995;142(1):1–8.
[76] Amphlett JC, Baumert RM, Mann RF, Peppley BA, Roberge PR, Harris TJ. Performance modeling of the Ballard Mark IV solid polymer electrolyte fuel cell (II. Empirical model development). J Electrochem Soc 1995;142(1):9–15.
[77] Amphlett JC, Mann RF, Peppley BA, Roberge PR, Rodrigues A. A model predicting transient responses of proton exchange membrane fuel cells. J Power Sources 1996;61:183–8.
[78] Mann RF, Amphlett JC, Hooper MAI, Jensen HM, Peppley BA, Roberge PR. Development and application of a generalized steady-state electrochemical model for a PEM fuel cell. J Power Sources 2000;86:173–80.
[79] Fowler MW, Mann RF, Amphlett JC, Peppley BA, Roberge PR. Incorporation of voltage degradation into a generalized steady state electrochemical model for a PEM fuel cell. J Power Sources 2002;106:274–83.
[80] EG&G Technical Services, Inc. Fuel Cell Handbook. US DOE: 2004.
[81] http://www.bcsfuelcells.com/24-Cell,%201kW%20Stack.htm .
[82] Mann RF, Amphlett JC, Peppley BA, Thurgood CP. Application of Butler–Volmer equations in the modeling of activation polarization for PEM fuel cells. J Power Sources 2006;161:775–81.
[83] Mann RF, Amphlett JC, Peppley BA, Thurgood CP. Henry's law and the solubilities of reactant gases of reactant gases in the modeling of PEM fuel cells. J Power Sources 2006;161:768–74.

[84] Mann RF, Amphlett JC, Peppley BA, Thurgood CP. Anode polarization on Pt(*h k l*) electrodes in dilute sulphuric acid electrolyte. J Power Sources 2007;163:679–87.
[85] Zhang J, Fisher TS, Ramchandran PV, Gore JP, Mudawar I. A review of heat transfer issues in hydrogen storage technologies. J Heat Transfer 2005;127:1391–9.
[86] David E. An overview of advanced materials for hydrogen storage. J Mater Process Technol 2005;162–163:169–77.
[87] Satyapal S, Petrovic J, Thomas G. Gassing up with hydrogen. Sci Am 2007:81–7.
[88] Sandi G. Hydrogen storage and its limitation. Electrochem Soc Interface 2004:40–4.
[89] Grochala W, Edwards PP. Thermal decomposition of the non-interstitial hydrides for the storage and production of hydrogen. Chem Rev 2004;104:1283–315.
[90] http://hydpark.ca.sandia.gov/PropertiesFrame.html.
[91] Vanhanen JP, Lund PD, Hagstrom MT. Feasibility study of a metal hydride hydrogen store for a self-sufficient solar hydrogen energy system. Int J Hydrogen Energy 1996;21(3):213–21.
[92] Vanhanen JP, Lund PD, Tolonen JS. Electrolyzer-metal hydride-fuel cell system for seasonal energy storage. Int J Hydrogen Energy 1998;23(4):267–71.
[93] Banerjee S, Murad S, Puri IK. Hydrogen storage in carbon nanostructures: possibilities and challenges for fundamental molecular simulations. Proc IEEE 2006;94(10):1806–14.
[94] Liu C, Fan YY, Liu M, Cong HT, Cheng HM, Dresselhaus MS. Hydrogen storage in single walled carbon nanotubes at room temperature. Science 1999;286:1127–9.
[95] ASHRAE handbook of fundamentals, 2005.
[96] http://corporate.honda.com/environment/fuel_cells.aspx?id = fuel_cells_fcx.
[97] Buildings energy data book. DOE, EERE; 2005.
[98] Fernandez JE. Materials for aesthetic, energy-efficient, and self diagnostic buildings. Science 2007;315: 1807–10.
[99] Moujaes S, Deshmukh SS. An evaluation of a residential energy conserving HVAC system and a residential energy demand/management system. Energy Eng J Assoc Energy Eng 2005;102(6):39–57.